Caving 2022 - Y Potvin (ed.)

doi:10.36487/ACG_repo/2205_84

Stress shadowing effects during hydraulic fracturing in block caving operations

C Mejia *Multiphysics Modelling and Simulation Group, Tecgraf Institute/PUC-Rio, Brazil*

E Azad *Universidad de Chile, Chile*

D Roehl *Pontifical Catholic University of Rio de Janeiro, Brazil*

JA Vallejos *Universidad de Chile, Chile*

E Rojas *Codelco, Chile*

Abstract

The hydraulic fracturing (HF) technique is mainly used to precondition the orebody before mining in the block caving extraction method. Weakening the rock mass to enhance its caveability, reduce seismic risks and reduce fragment sizes are the primary objectives of HF in mining. HF is used mainly in large-scale deep underground mines with low-grade metal orebodies. In this paper, hydraulic fracturing simulation is conducted based on the finite element method to study the effect of simultaneous and sequential multiple hydraulic fracturing schemes. The input and in situ data used for this simulation come from the El Teniente porphyry Cu-Mo mine. The fracture propagation is modelled with the cohesive elements using a traction-separation law. Comparing 3D and axisymmetric analysis, the similarity between fracture propagation shape and crack length prompted us to adopt axisymmetric analyses with reduced computational cost. Scenarios of simultaneous and sequential operations were analysed to consider the stress shadow effect, an understandable consequence of deformation during hydraulic fracturing. This comparison determined the fracture aperture, pore pressure, stress, and crack length. Due to the stress shadowing effect, different fracture lengths are observed. In addition, sequential injections have a subtler effect than simultaneous injections.

Keywords: *hydraulic fracturing, stress shadowing effect, cohesive element, hydro-mechanical coupling, block caving*

1 Introduction

Following the historical use of hydraulic fracturing (HF) to determine the state of stress at Rangely, Colorado (Haimson 1972) and its widespread application in the oil and gas industries as a stimulation technique, hydraulic fracturing was introduced into the mining sector in 1997 at Northparkes Mine (Van As & Jeffrey 2000). In cave mining, hydraulic fracturing has been utilised to precondition the rock mass, induce reactivation after cave arrests, and rockburst mitigation (Catalan et al. 2012; Dou et al. 2009; Jeffrey et al. 2001). Additionally, it has been used in coal mining to improve coal seam permeability, hard roof control, and enhance top coal caveability (He et al. 2016a; Jeffrey & Mills 2000; Puri et al. 1991; Sun et al. 2021).

In recent years, HF has become a popular preconditioning technique in mining operations like block caving (Brown 2007; Flores & Catalan 2019; Gonzalez et al. 2022; Hao et al. 2019; He et al. 2016a). This method involves producing and extending fractures in rocks by injecting a fluid under pressure into a borehole section. The fluid pressure creates tensile stresses in the rock at the borehole wall, causing fractures to start and extend to the far-field (Haimson & Cornet 2003). This technology enables the controlled caving of roof rock in coal mines and block caving in large low-grade deep metal mines by preconditioning the orebody before mining (Darling 2011). This method weakens the rock mass enhancing its caveability, reducing seismic risks and reducing fragment sizes. In hard rock cave mining, similar to hydraulic fracturing in the shale gas industry, boreholes are drilled from either the surface or subsurface excavations, depending on the target

zone and access. Multiple transverse fractures are produced along the boreholes. Typically, fractures with a size of about 30 metres in radius, and spacing of 1–2.5 m apart are developed in cave mining. The injection is generally conducted with a volume of 8 to 20 m^3 water without additives or proppants at a flow rate of 5–10 L/s (Adams & Rowe 2013; Bunger et al. 2011; Catalan et al. 2012; He 2017). Based on the different tectonic stress regimes (normal, strike-slip, and thrust fault) as illustrated in Figure 1, hydraulic fractures open in the direction of the minimum principal stress and propagate in the direction of the maximum principal stress.

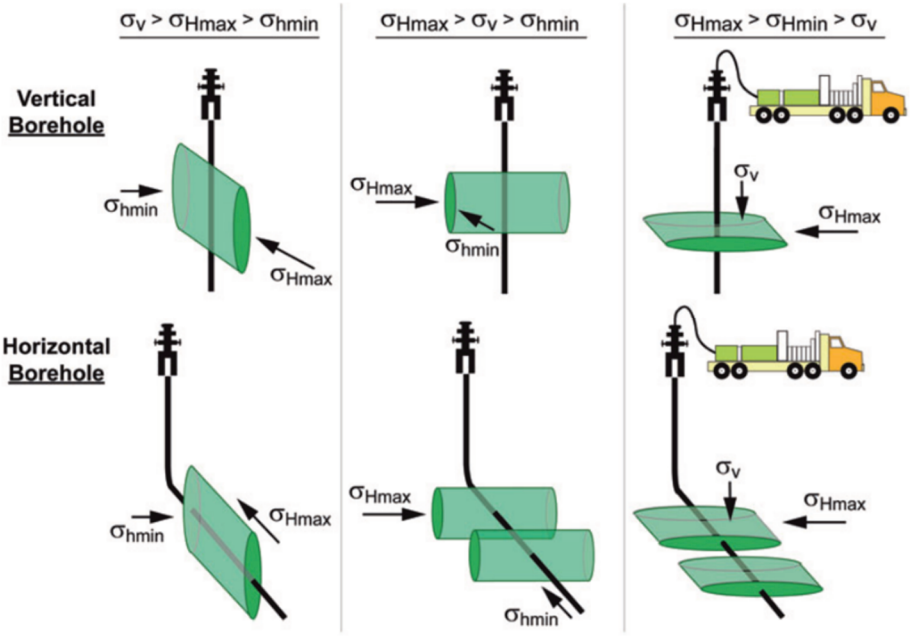

Figure 1 Relationship between hydraulic fracture opening and propagation directions relative to the in situ principal stresses, assuming these are aligned with vertical and horizontal (Eberhardt & Amini 2018)

For mining operations to reach the planned caveability, multiple simultaneous and/or sequential hydraulic fracturing operations are usually required. In the case of a fracture propagating through rock, both the changing dimensions in length and height along the leading edge and the changing width along the fracture extent cause a change in the stress field in the formation. Thus, when the stress acting on a rock mass changes, the rock mass will deform. Subsequently, if this same rock mass is deformed somehow, its stress field will change again. These stress changes induced by deformation caused by multiple simultaneous and sequential HF are known as Stress Shadow Effects (Geomechanics. LLC 2015; Han et al. 2021). The stress shadow effect may be dominated by the increase in minimum horizontal stress along the extent of the fracture. Still, a hydraulic fracture also induces other significant normal and shear stress changes.

Moreover, the increase in minimum horizontal stress will affect the trajectory of subsequent fractures that might propagate within the stress shadow region of a previous fracture. It may limit the response of adjacent hydraulic fractures in terms of tensile opening and hydraulic shearing (Preisig et al. 2015). Under the geotechnical conditions discussed in He et al. (2016a), orientation-uncontrolled fractures (e.g. orientations that are dictated by and are perpendicular to the minimum horizontal stress) would be unable to improve rock mass caveability and hence prevent desirable cave propagation.

Multiple cave mines with preconditioned rock masses are in operation. Northparkes Mine and Cadia East in Australia and Salvador, Andina, and El Teniente in Chile are the most substantial ones. Van As & Jeffrey (2000) presented the first use of HF for cave inducement at Northparkes block caving mine. In this mine, continuous caving stopped after the cave-back propagated to a maximum height of 95 m above the undercut and reverse faulting/in situ stress regime favoured the creation of horizontal fractures. In this study, various monitoring systems were utilised to evaluate fracture size, orientation, and rock mass quality, demonstrating that the

higher the number of fractures in the rock mass, the less effective the HF in preconditioning. Kaiser et al. (2013) and Catalan et al. (2012) discussed that in Cadia East Mine, the deepest panel caving mine in the world with thrust faulting stress condition, the combination of two preconditioning techniques was used. In the first phase, to introduce new joint sets to the rock mass, HF was conducted in boreholes (downholes) drilled from a subsurface excavation site above the targeted rock mass. Secondly, drilling and blasting boreholes (upholes) were drilled from the undercut level for further preconditioning of the hydraulically fractured rock mass and affecting its geomechanical parameters (Figure 2a) For some boreholes, their walls were prepared with an initial notch for HF initiation as trial. Due to time-consuming and unfavourable progress, since then, Cadia has not used notching as standard HF practice. This preconditioning combination was expected to lead to a cave propagation of around 110 mm/day, which was forecast to be 40% higher than expected without the preconditioning (estimated at a split of 25% by HF and 15% by blasting) (McTaggart et al. 2012).

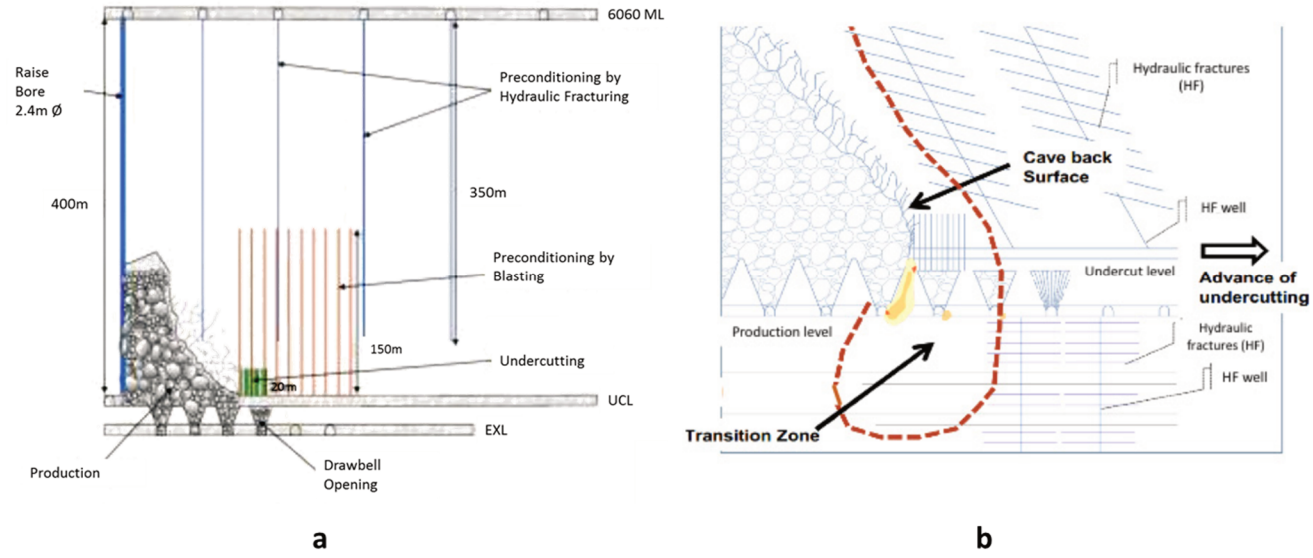

Figure 2 (a) Preconditioning by high undercut, hydraulic fracturing, blind blasting, and raisebored propagation, Cadia East Mine (McTaggart et al. 2012); (b) Conventional Panel Caving with HF at El Teniente Mine, Codelco (Rimmelin et al. 2020)

A full-scale HF trial at the Salvador mine revealed that, the initial notch is a powerful tool for managing HF initiation and avoiding undesirable paths.

In the presence of natural fractures of low permeable filling materials, fractures tend to cross rather than arrest at these natural fractures. However, distributed shear zones of lower shear strength and higher permeability significantly affected fracture propagation and acted as obstacles to propagation. The monitoring system in Salvador mine was used to identify the stress change and the influence of the stress shadowing effect on HF (He 2017; Puller et al. 2016). For 15 years, El Teniente mine has widely used hydraulic fracturing for preconditioning. It is now a fundamental element of its mining technique. Currently, hydraulic fracturing is used in conjunction with traditional undercutting to generate fractures every 1.5 m from the undercut upwards into the rock mass and downwards to the production level (Figure 2b). Studies showed that HF produces fracture propagation between 17 m and 30 m in a Dacite rock type, and the stress shadow effect is still significant in a range of 8 m to 15 m of fracture propagation (Brzovic et al. 2019; Rimmelin et al. 2020).

Small-scale laboratory experiments of Bunger et al. (2011) clearly showed the stress shadow effect caused the re-orientation of second and fourth fracture paths and unparallel propagation to Fractures 1 and 3 (Figure 3a). A 3D simulation conducted by Roussel & Sharma (2011) demonstrated the extent of stress reversal regions between two pre-existing fractures (Figure 3b). If a new fracture were initiated within the shaded area in Figure 3b, the fracture would initially propagate unparallel or even perpendicular to the original fracture and run aligned to the wellbore. Numerical modelling for directional hydraulic fractures in heterogeneous rock mass by He et al. (2016b) indicated that for the in situ stress regime in the heterogeneous

rock mass when the borehole lies in the σ_2–σ_3 plane, only the difference between σ_2 and σ_3 has a significant effect on fracture reorientation. Meanwhile, He et al. (2017) reported that, based on the results of a 3D numerical modelling code for homogeneous rock mass, both differential stresses (σ_1–σ_3 and σ_2–σ_3) have an impact on hydraulic fracture re-orientation. Hydraulic fracture re-orientation is unaffected by the magnitude of the minimum far-field stress. The homogeneity of the rock mass heavily influences fracture propagation before reorientation from its initiation point. Three-dimensional modelling simulating fracture propagation in simultaneous and sequential HF operations (Kumar & Ghassemi 2018) showed that the outer fractures dominate the growth of inner fractures in the concurrent propagation of hydraulic fractures. The stress shadowing region also causes the centre fractures to stop after reaching a certain length. An even more complex fracture network, as during block caving, will lead to a stronger interaction between fractures (hydraulic and natural fractures) due to a higher fracture density. This requires a more subtle consideration of stress shadowing during fracture simulations (Ma & Holditch 2015).

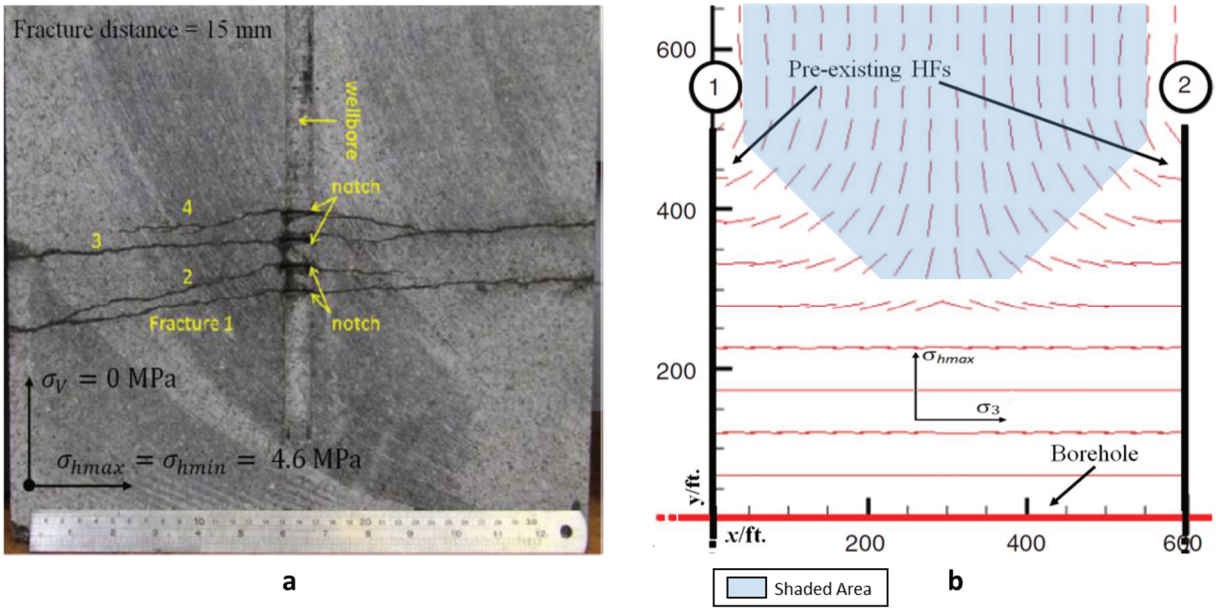

Figure 3 Stress shadowing effect. (a) HF trajectories demonstrate that the stress shadow effect is strong enough to induce HF re-orientation (Bunger et al. 2011); (b) Stress tensor distribution between two pre-existing HFs and the whole interval is occupied by the stress reversal region (Roussel & Sharma 2011)

To achieve a more realistic result in hydraulic fracturing simulation, hydro-mechanical (HM) coupling is required (Azad et al. 2018; Carrier & Granet 2012; Gao & Ghassemi 2020a). Changes in pore pressure generated by injection, in particular, influence the effective and total stresses in the reservoir and overburden in HM-coupled reservoir models. The hydraulic parameters of the reservoir, such as porosity and permeability, are affected by these stress variations. These, in turn, have an impact on fluid flow (Shojaei & Shao 2017). In geomechanics fields with complex geology, the Finite Element Method (FEM) despite all difficulties in fracture modelling and considerable computation cost, is still the most flexible and robust tool for handling complicated geometry, multiphysics coupling, and nonlinear deformation (Gao & Ghassemi 2020a).

Cohesive Zone Models (CZM) describe fracture initiation, propagation, and interaction with pre-existing natural fractures, with efficiency and powerful algorithms (Chen et al. 2021; Cordero et al. 2019; Rueda et al. 2020; Sanchez et al. 2020). This technique eliminates the physically unrealistic singularity in the crack tip stress field present in linear elastic fracture mechanics and offers an effective alternative to analyse fracture behaviour quantitatively via simulation of the fracture processes (Gao & Ghassemi 2020b; Shojaei & Shao 2017). Sanchez et al. (2020) used CZM in 3D numerical models to study hydraulic fracture propagation and its interaction with pre-existing natural fractures. The results indicate that in situ stresses and the angle of

approach between hydraulic fracture and natural fracture are the most significant factors affecting fracture interaction. Moreover, Basson et al. (2021) developed a fully coupled 3D Material Point Method as a meshless tool for simulating HF preconditioning in realistic mining situations. Their work depicts that HF is an ideal alternative for preconditioning high stress rock mass when there is a significant difference between the principal stresses in a material. The paper by Cordero et al. (2019) presented an innovative methodology of mesh fragmentation to insert the special triple-noded interface elements into FEM combined with a CZM to simulate nonlinear coupling processes of hydraulic fracture propagation naturally fractured media.

Jamaloei (2021) compares various HF modelling techniques by considering the critical factors that influence the hydro-fracturing process, including injection rate, crack opening and geometry determination, proppant movement, interaction with natural fractures, stress shadowing effect, stress-field dependency, and so on. The comparisons revealed that continuum and extended continuum-based models, such as FEM and extended-FEM, are the best options for HF modelling in large-scale problems. Escobar et al. (2019) applied a HM extended-FEM model to investigate the effect of simultaneous and sequential multiple hydraulic fracturing schemes on fracture geometry. Chen et al. (2021) reviewed different commercial software for hydraulic fracturing design, such as Elfen, FracMan, and XSite, which are equipped with field injection pressure and microseismic events and focus on practicability and efficiency of the simulation. These HF modelling software packages include modules for data analysis, automatic pump scheduling, post-fracture production analysis, and more. A process from log analysis to production prediction can be developed using these modules.

This paper studies the influence of simultaneous and sequential multiple hydraulic fracturing schemes using a fully coupled HM simulation of HF based on the FEM. The theoretical background for fluid-driven fracture propagating in a permeable poroelastic media is discussed. The rock formation is represented using a fully coupled HM continuum element. In the same way, a fully coupled HM interface element models fracture behaviour. Fracture propagation is governed by a CZM. Then model geometry, properties, and field data are presented. The input and in situ data used for this simulation come from the El Teniente porphyry Cu-Mo mine. 3D and axisymmetric models are compared in fracture propagation shape and crack length. To consider the influence of the stress shadow effect as the most observable result of deformation during HF, two simultaneous and sequential HF operation scenarios are studied. The comparison considers fracture aperture, pore pressure, stress change, and crack length.

2 Methodology

HF involves several coupling processes such as fracture propagation, fluid flow inside the fracture channels, and fluid migration through a deformable porous medium. The governing equations of these processes are summarised as follows.

2.1 Governing equation of porous media

The formulation presented in this work considers an isotropic, linear elastic medium undergoing small strains. Biot's theory is adopted to model the saturated porous media. The conservation of the linear momentum in the saturated porous media takes the form:

$$\nabla \cdot \boldsymbol{\sigma} + \rho\, \boldsymbol{g} = 0 \tag{1}$$

where:

- $\boldsymbol{\sigma}$ = stress tensor.
- ρ = density of the saturated porous medium.
- $\boldsymbol{g}$ = gravity vector.

The relationship between total stresses and effective stresses in porous media is given by:

$$\boldsymbol{\sigma}' = \boldsymbol{\sigma} - \alpha\, \boldsymbol{p} \tag{2}$$

here:

$\boldsymbol{\sigma}'$ = effective stress tensor (compression is negative hereafter).

$\boldsymbol{p}$ = pore pressure.

α = Biot coefficient which is defined as:

$$\alpha = 1 - K/K_s \quad (3)$$

where:

K and K_s are the volumetric deformation moduli of the porous medium and solid grain, respectively.

For incompressible solid grains, observe that $K_s \to \infty$ and $\alpha = 1$. The constitutive relation in the bulk material is given by:

$$\boldsymbol{\sigma} = \mathbf{D}_{\mathrm{e}} : \boldsymbol{\varepsilon} \quad (4)$$

where:

$\boldsymbol{\varepsilon}$ = strain vector.

$\boldsymbol{D}_e$ = elasticity matrix.

Considering small volumetric strain, the mass balance equation of the pore fluid is:

$$\frac{1}{M}\,\dot{\boldsymbol{p}} + \alpha \nabla \dot{\boldsymbol{u}} + \nabla \boldsymbol{v} = 0 \quad (5)$$

where:

$\boldsymbol{v}$ = pore fluid velocity.

M = Biot's modulus:

$$M = \left\{ \frac{\phi_o}{K_f} + \frac{\alpha - \phi_o}{K_s} \right\}^{-1} \quad (6)$$

where:

K_f = bulk modulus of the pore fluid.

ϕ_o = initial porosity.

Under isothermal conditions, laminar fluid flow through the porous media can adopt Darcy's law as follow:

$$\boldsymbol{v} = -\frac{\boldsymbol{k}}{u_f} \nabla p \quad (7)$$

where:

$\boldsymbol{k}$ = permeability tensor.

u_f = dynamic fluid viscosity.

2.2 Governing equation of fractures

The hydro-mechanical behaviour of induced fractures includes fracture propagation and fluid flow inside the fracture channels. As presented by Potts et al. (2001), the shear stress τ_s and normal stress σ_n on the fracture surface are related to their corresponding relative displacement across the crack surface Δ_s and Δ_n according to:

$$\begin{bmatrix} \tau_s \\ \sigma_n \end{bmatrix} = \begin{bmatrix} K_s & 0 \\ 0 & K_n \end{bmatrix} \begin{bmatrix} \Delta_s \\ \Delta_n \end{bmatrix} \quad (8)$$

where:

K_n and K_s stand for the normal and shear elastic stiffness, respectively.

The degradation process begins when the following quadratic damage initiation criterion is satisfied:

$$\left(\frac{\langle\sigma_n\rangle}{\sigma_{no}}\right)^2 + \left(\frac{\tau_s}{\tau_{so}}\right)^2 = 1 \quad (9)$$

where:

$\langle\bullet\rangle$ = Macaulay brackets.

σ_{no} and τ_{so} are the rock normal and shear strength, respectively

The damage evolution law governs the degradation process at the fracture tip as follows:

$$\begin{bmatrix}\tau_s \\ \sigma_n\end{bmatrix} = (1-d)\begin{bmatrix}\tau_s^* \\ \sigma_n^*\end{bmatrix} - dD_e\begin{bmatrix}0 \\ \langle-\Delta_n\rangle\end{bmatrix} \quad (10)$$

where:

d = scalar damage variable.

τ_s^* and σ_n^* = trial stress components obtained by the linear elastic constitutive model.

The scalar damage variable evolves from zero at damage initiation, to one, the maximum damage value, when the material is completely damaged. Figure 4 illustrates the typical response of the damage model with linear softening (Turon et al. 2006).

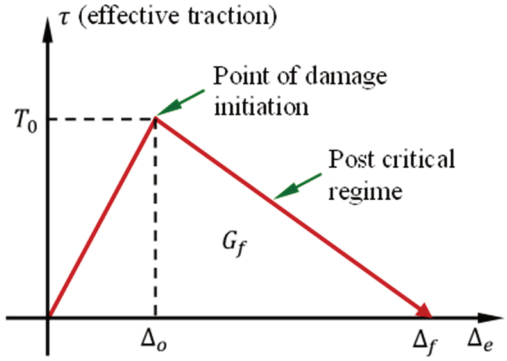

Figure 4 Schematic representation of the cohesive model with linear softening

Fluid flow inside the fracture channels occurs in the longitudinal and normal directions according to:

$$\frac{\partial\Delta_n}{\partial t} + \frac{\partial q_l}{\partial s} + q_T + q_B = q_w \quad (11)$$

where:

Δ_n = normal fracture aperture.

q_l = longitudinal flow rate.

s = longitudinal coordinate along the fracture.

q_T and q_B = normal fluid flow leaking into the rock formation.

Figure 5 shows the fluid flow pattern inside the induced fracture.

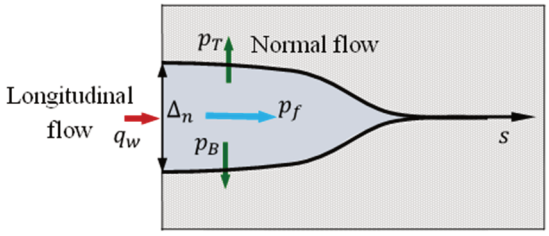

Figure 5 Fluid flow pattern inside the fracture channel

Assuming incompressible and Newtonian fluid, the cubic law of parallel plates governs the longitudinal flow rate that is defined as:

$$q_l = \frac{\Delta_n^3}{12u_f}\frac{\partial p_f}{\partial s} \tag{12}$$

where:

u_f = dynamic fluid viscosity.

p_f = fluid pressure inside the fracture.

3 Parameters and numerical model

This section presents the geometry and parameters adopted to study the stress shadowing effect on the preconditioning of a synthetic block caving operation. Two different configurations are adopted to model the HF propagation, as shown in Figure 6. The geometry, boundary, and load conditions adopted by the 3D and axisymmetric models are illustrated in Figure 6. The 3D model is discretised using 48,373 nodes, 39,600 stress/pore fluid continuum elements, and 3,600 stress/fluid interface elements. On the other hand, the axisymmetric model is discretised using 36,491 nodes, 32,000 stress/pore fluid axisymmetric elements, and 400 stress/fluid axisymmetric interface elements. The interface elements are placed perpendicular to the minimum principal stress (σ_v) that represents the fracture path.

The rock formation is assumed to be initially saturated and under in situ stresses of σ_{v0} = 20.9 MPa, σ_{H0} = 58.8 MPa, and σ_{h0} = 34.9 MPa. All simulations consider fracture initiation based on the maximum principal stress (3.1 MPa), and material degradation process governed by linear softening adopting fracture energy of 0.5 kPa/m. A Newtonian fluid with a dynamic viscosity of 1.0 cP and a specific fluid weight of 10 kPa/m is injected at a constant rate of q_w = 0.0063 m^3/s during 41 min.

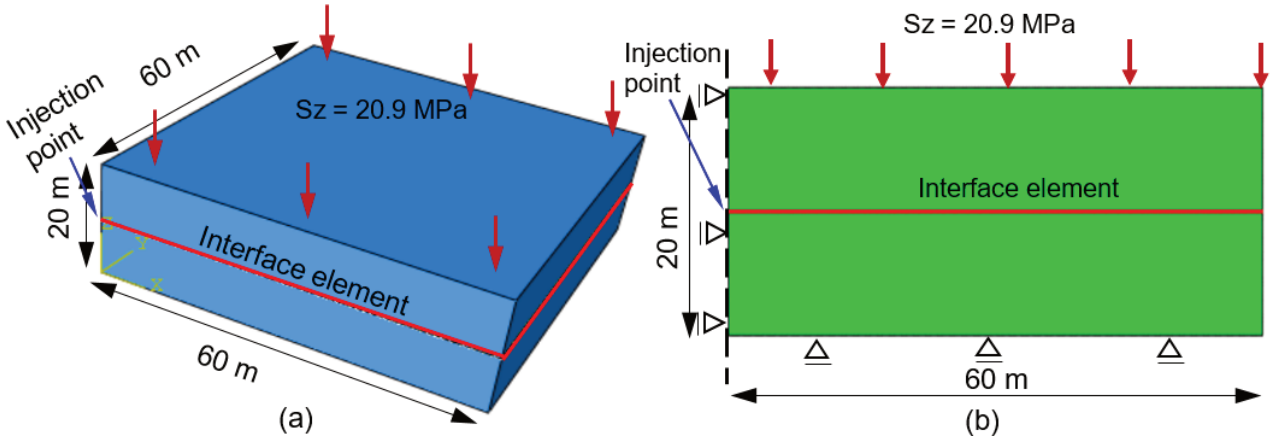

Figure 6 Schematic representation of (a) 3D and (b) axisymmetric configurations

Table 1 summarises the properties of the andesite rock, hydraulic fracture, and injection fluid adopted in all simulations. The rock properties adopted are representative of the El Teniente mine. A poroelastic constitutive model represents the rock matrix behaviour, while the fracture degradation process follows the cohesive zone model.

Table 1 Hydraulic and mechanical properties

Category	Parameter	Unit	Value
Rock matrix	Young modulus (E)	GPa	53
	Poisson's ratio (v)	–	0.19
	Hydraulic conductivity (k)	m/s	2e-8
	Porosity (ϕ)	%	1.46
	Void ratio (η)	–	0.0171
Hydraulic fracturing	Tensile strength	MPa	3.1
	Normal stiffness	GPa/m	6.00 E+04
	Shear stiffness	GPa/m	6.00 E+04
	Fracture energy	kN/m	0.5
	Leak-off	m/kPa*s	6.00 E-10
	Initial gap	m	1.00E-03
Injection fluid (water)	Injection rate	m^3/s	0.0063
	Fluid viscosity	Pa*s	0.001
	Injection time	Min	41

Figure 7 exhibits the numerical model adopted to study the stress shadowing effect considering simultaneous and sequential hydraulic fracturing. This model consists of five axisymmetric induced fractures propagating in a poroelastic formation. Interface elements are placed along horizontal paths with 2 m of fracture spacing in which the fractures are expected to propagate.

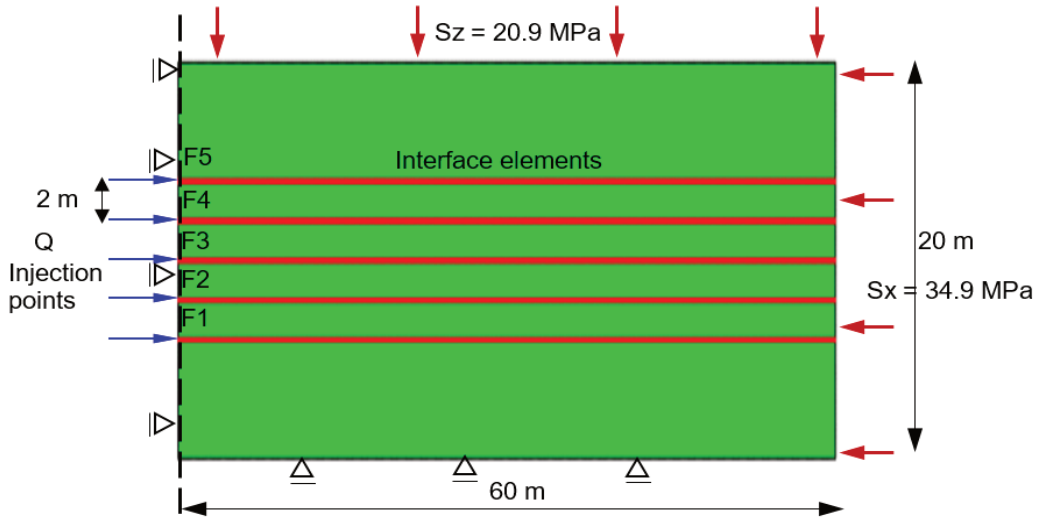

Figure 7 Schematic representation of axisymmetric model with multiple fracture paths

The geometry, boundary, and load condition are the same as in the previous model. The fractures are stimulated simultaneously or injected sequentially, one after the other. Each fracture is stimulated by injecting fracturing fluid (water) for 41 min.

4 Discussion and results

This section presents a comparison between the axisymmetric and 3D numerical models. Later, the stress shadowing effect induced by simultaneous and sequential hydraulic fracturing schemes is also discussed.

4.1 Comparison between 3D and axisymmetric models

Considering the in situ stress of σ_{v0} = 20.9 MPa, σ_{H0} = 58.8 MPa, and σ_{h0} = 34.9 MPa, the induced fracture propagates on the horizontal plane as expected, perpendicularly to the minimum in situ stress σ_{v0}. Figure 8 shows the fracture geometry and pore pressure field after 41 min of injection.

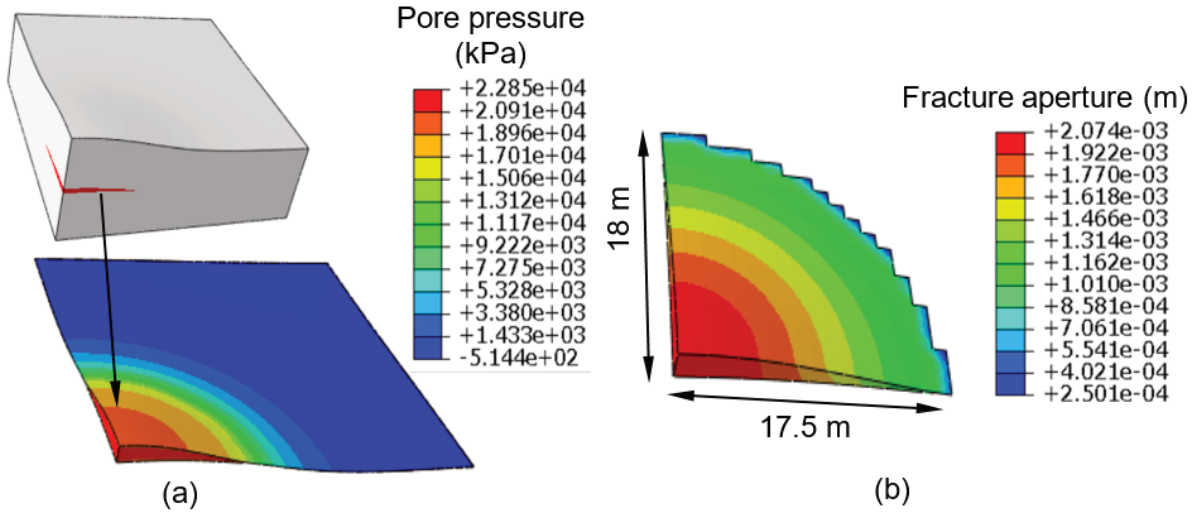

Figure 8 Induced fracture after 41 min of injection (a) pore pressure field and (b) fracture aperture

Figure 9 shows the minimum in situ stress (σ_{zz}) and pore pressure at the final configuration after 41 min of injection. The stresses inside the fracture are tractive (positive), while the stresses in the rock formation are compressive (Figure 9a). Figure 9b shows the fluid migration through the rock formation.

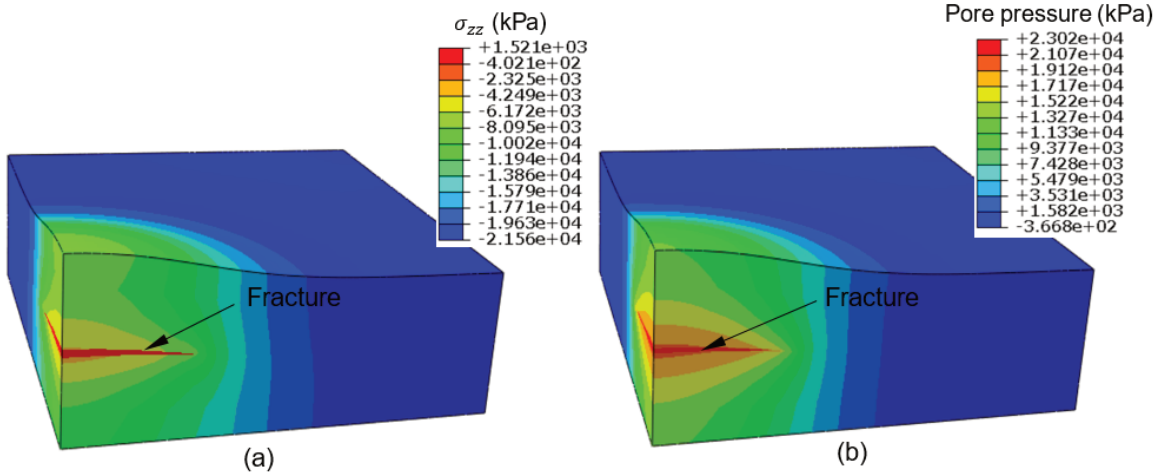

Figure 9 Numerical results after 41 min of injection (a) Vertical stresses and (b) Pore pressure field

Figure 10 compares the fracture geometry obtained using axisymmetric and 3D models. For symmetry, the 3D model shows one quarter of the fracture geometry while the axisymmetric model shows half of the fracture geometry. Notice that both models propagate near 17.0 m with a circular shape after 41 min of injection.

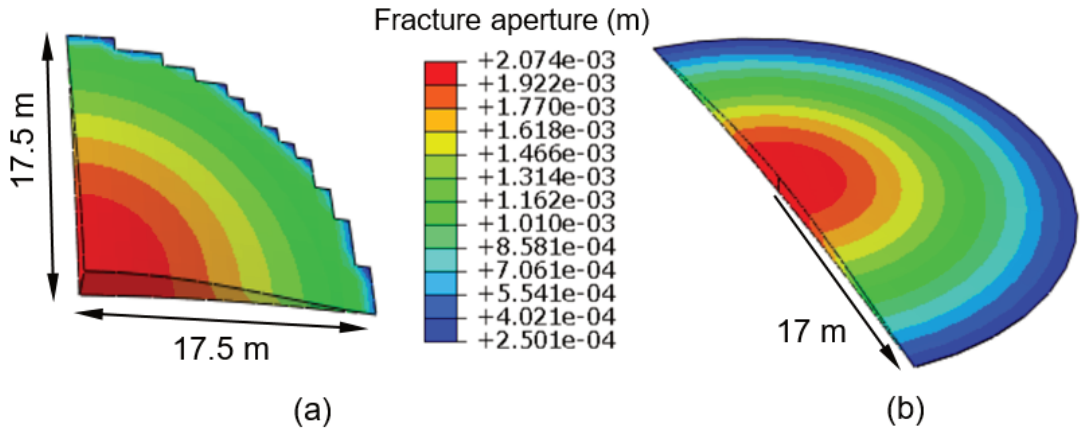

Figure 10 Comparison of the fracture length between (a) 3D and (b) Axisymmetric models

According to the numerical results, the axisymmetric model generates the same geometry with lower computational time. Therefore, the axisymmetric model is adopted to study the stress shadowing effect for different fracturing schemes.

4.2 Simultaneous HF scheme

In a simultaneous HF scheme, the injection of all fractures happens at the same time. Although the sequential scheme is adopted in real applications, the simultaneous fracturing scheme is investigated to evaluate the efficiency of the rock mass preconditioning. Figure 11 shows the final fracture lengths of each fracture after 41 min of injection. Notice that different fracture lengths are observed due to the stress shadowing effect. Fractures F1 and F2 are shorter because they are affected by the stress shadowing induced by fractures F3, F4, and F5. As a result, fractures F1 and F2 have larger fracture aperture because they are injected with the same fluid volume. For the boundary conditions adopted, fractures F3 and F4 have the same fracture lengths (approximately 34 m) and F5 is longer (52 m) with a small fracture aperture.

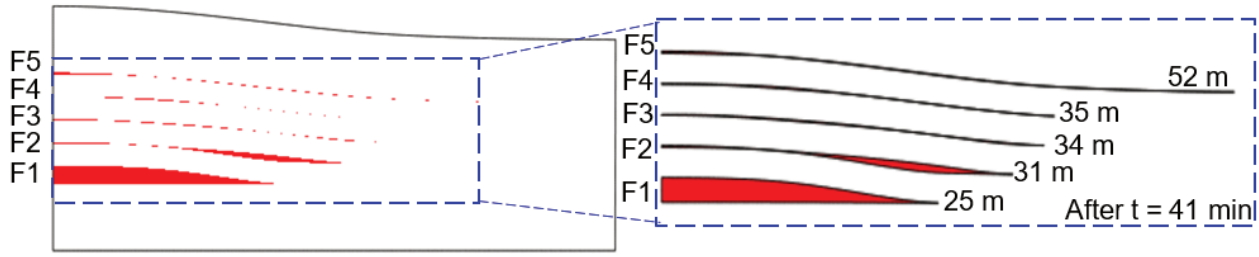

Figure 11 Fracture lengths for simultaneous HF scheme after 41 min of injection

Figure 12 shows the fracture geometry and pore pressure field after 41 min of injection. Notice that fractures F1 and F2 are shorter with a larger aperture and a higher fluid pressure inside the fracture. On the other hand, fracture F5 is larger with lower fluid pressure. These results are expected because the fracture propagation is constrained to happen in a predefined path. However, the fracture paths can deviate in a real application due to the stress shadowing effect.

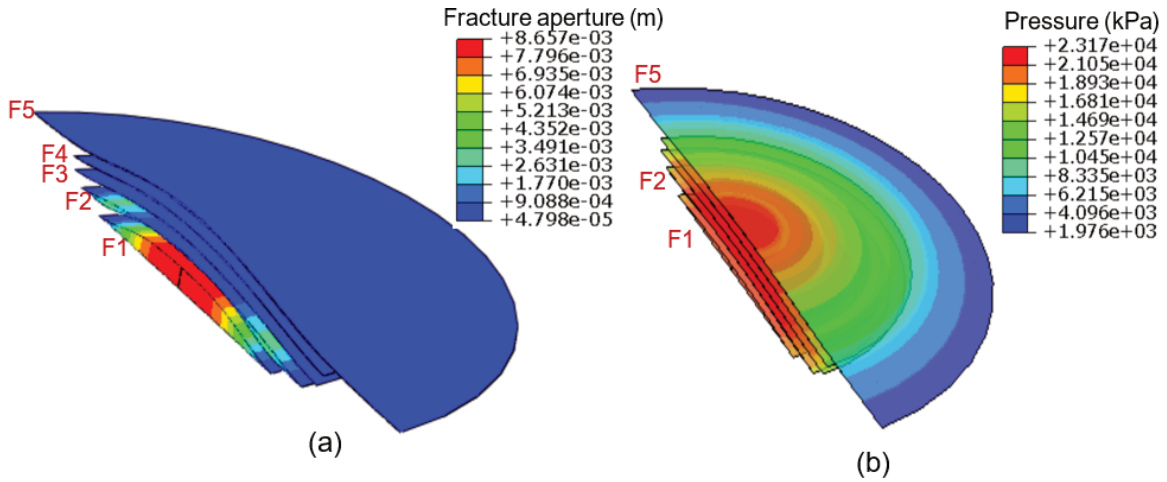

Figure 12 Numerical results after 41 min of injection (a) Fracture aperture and (b) Pore pressure field

4.3 Sequential HF scheme

In a sequential fracturing scheme, fracture stimulation happens one after the other. The same fluid volume is injected inside each fracture. Figure 13 illustrates the final fracture length after 164 min (injection of 41 min for each fracture). Notice that the last fracture (F5) is larger with a higher fracture aperture due to the stress shadowing effect. In addition, the propagation of the last fracture closes the previous ones.

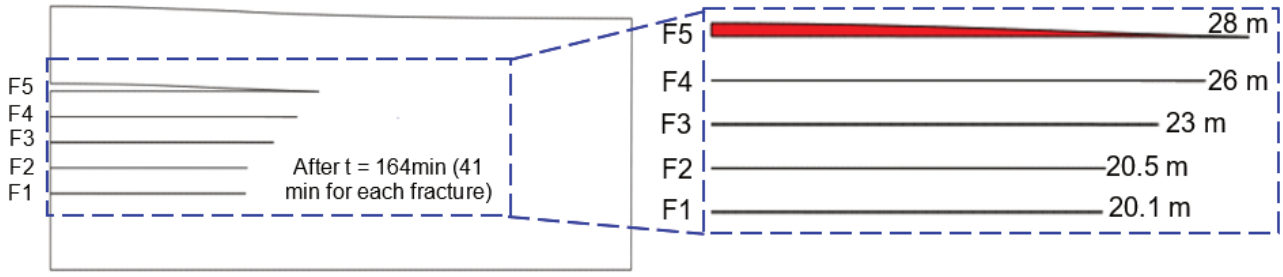

Figure 13 Fracture lengths considering sequential HF scheme

Figure 14 shows the fracture aperture and pore pressure field after 164 min, corresponding to 41 min of injection in each fracture. The fracture aperture of fracture F5 is larger than in the previous case due to the higher fluid pressure inside the fracture channels.

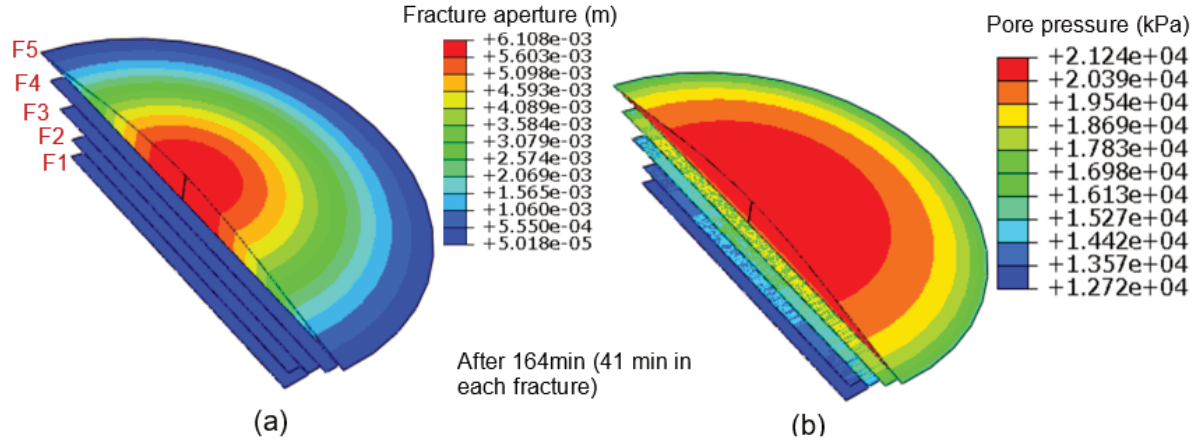

Figure 14 Numerical results after 164 min of injection (a) Fracture aperture and (b) Pore pressure field

Figure 15 illustrates the fracture aperture after the injection of each fracture. Figure 15a shows a small fracture aperture for fracture F1. The injection of fracture F2 reaches higher fluid pressure to close F1.

Consequently, the fracture aperture and length of F2 are larger. The same behaviour is observed during the injection of the subsequent fractures. Finally, as the fractures are stimulated, they require a high fluid pressure to propagate. As a consequence, their apertures are higher.

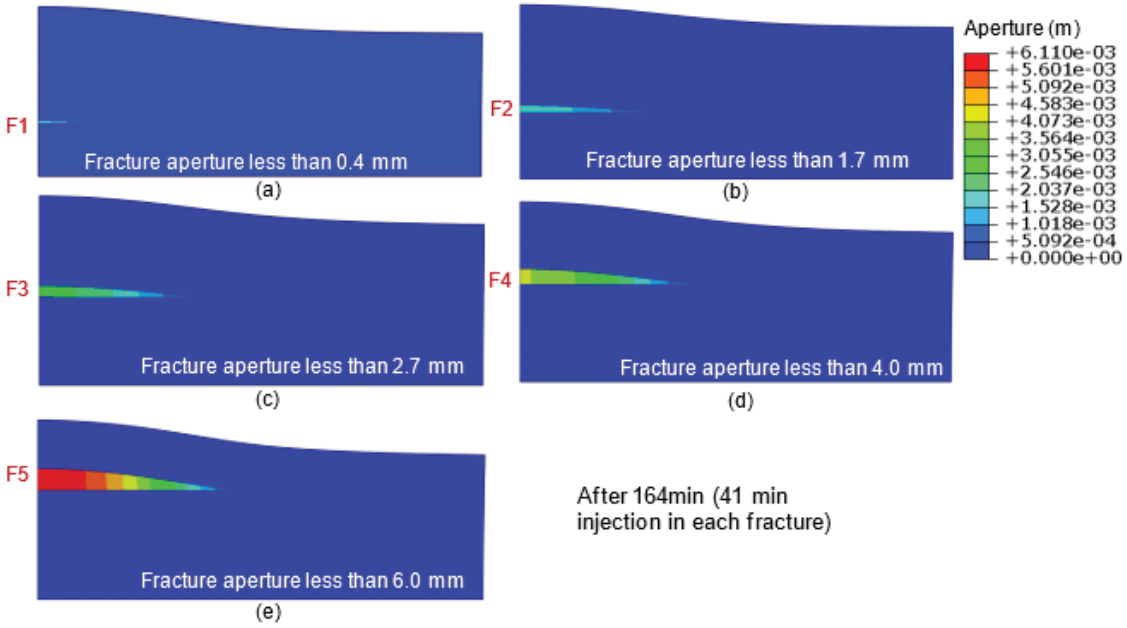

Figure 15 Fracture aperture after injection of fracture (a) F1, (b) F2, (c) F3, (d) F4, and (e) F5

5 Conclusion

This paper presents the numerical modelling of preconditioning rock mass by HF. The induced fractures are simulated using stress/fluid interface elements. These interface elements are placed along the paths in which the fractures are expected to propagate. However, the fracture path cannot be estimated in advance because it is affected by the stress shadow during the fracture process. The stress shadowing effect considering simultaneous and sequential HF schemes is investigated. In simultaneous HF, a competition of fracture propagations is observed. The propagation of some fractures interrupts the propagation of others. In the sequential fracturing scheme, the injection of new fractures closes the previous one. Consequently, the aperture of the new fractures is larger than the previous one due to the stress shadowing effect. The simultaneous HF scheme induces higher stress shadowing than the sequential one. According to the numerical results, the simultaneous scheme results in more extensive fractures, which are more beneficial to preconditioning hard rock caving mines. Finally, the intense stress shadowing effect between fractures can be induced and intensified by the predefined paths of the multiple fractures.

Acknowledgement

The authors gratefully acknowledge the support from the Brazilian Funding Agency: Brazilian National Council for Scientific and Technological Development (CNPq) process 309384/2019–2 and Fundação Carlos Chagas Filho de Amparo à Pesquisa do Estado do Rio de Janeiro (FAPERJ) – process E-26/202.928/2019. We also acknowledge the support from the Chilean National Agency for Research and Development (ANID) – 21212200, Beca de Doctorado Nacional 2021 and the basal CONICYT project AFB180004 of the Advanced Mining Technology Center (AMTC) – University of Chile.

References

Adams, J & Rowe, C 2013, 'Differentiating applications of hydraulic fracturing', paper presented at the *ISRM International Conference for Effective and Sustainable Hydraulic Fracturing.*

Azad, E, Peik, B & Abbasi, B 2018, 'A numerical simulation of thermo-mechanical behaviour of a single fracture in porous rock', paper presented at the *52nd US Rock Mechanics/Geomechanics Symposium.*

Basson, G, Bassom, A P & Salmon, B 2021, 'Simulating hydraulic fracturing preconditioning in mines with the material point method', *Journal of Applied Geophysics*, vol. 195, 104471.

Brown, E 2007, 'Rock mechanics-the basic mining science: challenges in underground mass mining', Paper presented at the *11th ISRM Congress.*

Brzovic, A, Celhay, F, Gonzalez, R & Hurtado, J 2019, 'Evidence of a consistent process of rock fracturing during material flow within ore columns – 25 Years of fragmentation experience at the El Teniente Mine', paper presented at the *53rd US Rock Mechanics/Geomechanics Symposium.*

Bunger, A, Jeffrey, R, Kear, J, Zhang, X & Morgan, M 2011, 'Experimental investigation of the interaction among closely spaced hydraulic fractures', paper presented at the *45th US Rock Mechanics/Geomechanics Symposium.*

Carrier, B & Granet, S 2012, 'Numerical modelling of hydraulic fracture problem in permeable medium using cohesive zone model', *Engineering Fracture Mechanics*, vol. 79, pp. 312–328.

Catalan, A, Dunstan, G, Morgan, M, Green, S, Jorquera, M, Thornhill, T, … Chitombo, G 2012, 'How can an intensive preconditioning concept be implemented at mass mining method? Application to Cadia East panel caving project', paper presented at the *46th US Rock Mechanics/Geomechanics Symposium.*

Chen, B, Barboza, B R, Sun, Y, Bai, J, Thomas, H R, Dutko, M, … Li, C 2021, 'A review of hydraulic fracturing simulation', *Archives of Computational Methods in Engineering*, https://doi.org/10.1007/s11831-021-09653-z

Cordero, J A R, Sanchez, E C M & Roehl, D 2019, 'Hydromechanical modelling of unrestricted crack propagation in fractured formations using intrinsic cohesive zone model', *Engineering Fracture Mechanics*, 221, 106655.

Darling, P 2011, *SME Mining Engineering Handbook*, vol. 1, Society for Mining, Metallurgy & Exploration, Englewood.

Dou, L-M, Lu, C-P, Mu, Z-L & Gao, M-S 2009, 'Prevention and forecasting of rock burst hazards in coal mines', *Mining Science and Technology (China)*, vol. 19, no. 5, pp. 585–591.

Eberhardt, E & Amini, A 2018. Hydraulic Fracturing. In P Bobrowsky & B Marker (Eds.), *Encyclopedia of Engineering Geology,* pp. 1–6. Springer International Publishing, Cham.

Escobar, R G, Sanchez, E C M, Roehl, D & Romanel, C 2019, 'Xfem modelling of stress shadowing in multiple hydraulic fractures in multi-layered formations', *Journal of Natural Gas Science and Engineering*, vol. 70, 102950.

Flores, G & Catalan, A 2019, 'A transition from a large open pit into a novel 'macroblock variant' block caving geometry at Chuquicamata mine, Codelco Chile', *Journal of Rock Mechanics and Geotechnical Engineering*, 11(3), 549–561.

Gao, Q & Ghassemi, A 2020a, 'Finite element simulations of 3D planar hydraulic fracture propagation using a coupled hydro-mechanical interface element', *International Journal for Numerical and Analytical Methods in Geomechanics*, vol. 44, no. 15, pp. 1999–2024.

Gao, Q & Ghassemi, A 2020b, 'Three dimensional finite element simulations of hydraulic fracture height growth in layered formations using a coupled hydro-mechanical model', *International Journal of Rock Mechanics and Mining Sciences*, vol. 125, 104137.

Geomechanics LLC 2015, *Stress Shadows Explained: What It Is, What It Isn't, And Why You Should Care*, https://ofgeomech.com/ofg20/wp-content/uploads/2015/10/Stress_Shadows_Explained.pdf

Gonzalez, F, Vallejos, J, Rojas, E & Landeros, P 2022, 'Evaluation of the seismic rock mass response to mining and the impact of preconditioning using an epidemic-type aftershock model', *International Journal of Rock Mechanics and Mining Sciences*, vol. 150, 104975.

Haimson, B & Cornet, F 2003, 'ISRM suggested methods for rock stress estimation—part 3: hydraulic fracturing (HF) and/or hydraulic testing of pre-existing fractures (HTPF)', *International Journal of Rock Mechanics and Mining Sciences*, 40(7–8), 1011–1020.

Haimson, B C 1972, 'Earthquake related stresses at Rangely, Colorado', Paper presented at *The 14th US Symposium on Rock Mechanics (USRMS).*

Han, W, Cui, Z & Zhu, Z 2021, 'The Effect of Perforation Spacing on the Variation of Stress Shadow', *Energies*, vol. 14, no. 13, 4040.

Hao, C, Cheng, Y, Wang, L, Liu, H & Shang, Z 2019, 'A novel technology for enhancing coalbed methane extraction: hydraulic cavitating assisted fracturing', *Journal of Natural Gas Science and Engineering*, vol. 72, 103040.

He, Q 2017, *Creating Prescribed Hydraulic Fractures in Cave Mining*, doctoral dissertation, University of New South Wales, Australia.

He, Q, Suorineni, F & Oh, J 2016a, 'Review of hydraulic fracturing for preconditioning in cave mining', *Rock Mechanics and Rock Engineering*, 49(12), 4893–4910.

He, Q, Suorineni, F, Oh, J & Ma, T 2016b, 'Modeling directional hydraulic fractures in heterogeneous rock masses', *MassMin, Sydney*.

He, Q, Suorineni, F T, Ma, T & Oh, J 2017, 'Effect of discontinuity stress shadows on hydraulic fracture re-orientation', *International Journal of Rock Mechanics and Mining Sciences*, vol. 91, pp. 179–194.

Jamaloei, B Y 2021, 'A critical review of common models in hydraulic-fracturing simulation: A practical guide for practitioners', *Theoretical and Applied Fracture Mechanics*, 113, 102937.

Jeffrey, R & Mills, K 2000, 'Hydraulic fracturing applied to inducing longwall coal mine goaf falls', Paper presented at the *4th North American rock mechanics symposium.*

Jeffrey, R, Zhang, X, Settari, A, Mills, K & Detournay, E 2001, 'Hydraulic fracturing to induce caving: fracture model development and comparison to field data', Paper presented at the *DC Rocks 2001, The 38th US Symposium on Rock Mechanics (USRMS).*

Kaiser, P K, Valley, B, Dusseault, M B & Duff, D 2013, 'Hydraulic fracturing mine back trials—design rationale and project status', paper presented at the *ISRM International Conference for Effective and Sustainable Hydraulic Fracturing.*

Kumar, D & Ghassemi, A 2018, 'Three-dimensional poroelastic modelling of multiple hydraulic fracture propagation from horizontal wells', *International Journal of Rock Mechanics and Mining Sciences*, 105, 192–209.

Ma, Y Z & Holditch, S 2015, *Unconventional Oil and Gas Resources Handbook: Evaluation and development*, Gulf Professional Publishing.

McTaggart, P, Slifirski, M, Shillaker, M, Kronborg, M, Webb, S, Gurry, J, … Shah, N 2012, *Block Caving with Rio and NCM*, viewed 12/7/2022, https://bit.ly/3yRJdG3

Potts, D M, Zdravković, L, Addenbrooke, T I, Higgins, K G & Kovačević, N 2001, *Finite Element Analysis in Geotechnical Engineering: Application*, vol. 2, Thomas Telford, London.

Preisig, G, Eberhardt, E, Gischig, V, Roche, V, van der Baan, M, Valley, B, … Lowther, R 2015, 'Development of connected permeability in massive crystalline rocks through hydraulic fracture propagation and shearing accompanying fluid injection', *Geofluids*, vol. 15, no. 1–2, pp. 321–337.

Puller, J W, Mills, K W, Jeffrey, R G & Walker, R J 2016, 'In-situ stress measurements and stress change monitoring to monitor overburden caving behaviour and hydraulic fracture pre-conditioning', *International Journal of Mining Science and Technology*, vol. 26, no. 1, pp. 103–110.

Puri, R, King, G & Palmer, I 1991, 'Damage to coal permeability during hydraulic fracturing', paper presented at the *Low Permeability Reservoirs Symposium.*

Rimmelin, R, Chitombo, G & Rojas, E 2020, 'Hydraulic fracturing in cave mining: Opportunities for improvement', Paper presented at the *MassMin 2020: Proceedings of the Eighth International Conference & Exhibition on Mass Mining.*

Roussel, N P & Sharma, M M 2011, 'Optimizing fracture spacing and sequencing in horizontal-well fracturing', *SPE Production & Operations*, vol. 26, no. 02, pp. 173–184.

Rueda, J, Mejia, C, Quevedo, R & Roehl, D 2020, 'Impacts of natural fractures on hydraulic fracturing treatment in all asymptotic propagation regimes', *Computer Methods in Applied Mechanics and Engineering*, 371, 113296.

Sanchez, E C M, Cordero, J A R & Roehl, D 2020, 'Numerical simulation of three-dimensional fracture interaction', *Computers and Geotechnics*, 122, 103528.

Shojaei, A & Shao, J 2017, *Porous Rock Fracture Mechanics: With Application to Hydraulic Fracturing, Drilling and Structural Engineering*, Woodhead Publishing.

Sun, Y, Fu, Y & Wang, T 2021, 'Field application of directional hydraulic fracturing technology for controlling thick hard roof: a case study', *Arabian Journal of Geosciences*, vol. 14, no. 6, pp. 1–15.

Turon, A, Camanho, P P, Costa, J & Dávila, C 2006, 'A damage model for the simulation of delamination in advanced composites under variable-mode loading', *Mechanics of materials*, 38(11), 1072–1089.

Van As, A & Jeffrey, R 2000, 'Caving induced by hydraulic fracturing at Northparkes mines', Paper presented at the *4th North American Rock Mechanics Symposium.*